International Journal of Pressure Vessels and Piping 146 (2016) 203–215

Contents lists available at ScienceDirect

International Journal of Pressure Vessels and Piping

journal homepage: www.elsevier.com/locate/ijpvp

Thermo-mechanical behaviour during encapsulation of glass in a steel vessel

S. Nakhodchi [a, *], D.J. Smith [b], B.G. Thomas [c]

[a] Faculty of Mechanical Engineering, K. N. Toosi University of Technology, Tehran, Iran
[b] Department of Mechanical Engineering, University of Bristol, UK
[c] Department of Mechanical and Industrial Engineering, University of Illinois, Urbana-Champaign, USA

ARTICLE INFO

Article history:
Received 2 October 2015
Received in revised form
3 June 2016
Accepted 3 July 2016
Available online 5 July 2016

Keywords:
Thermo-mechanical process
Finite element
Residual stress

ABSTRACT

Quantitative numerical simulations and qualitative evaluations are conducted to elucidate thermo-mechanical behaviour during pouring and solidification of molten glass into a stainless-steel cylindrical container. Residual stress and structural integrity in this casting/vitrification process is important because it can be used for long-term storage of high-level nuclear wastes. The predicted temperature and stress distributions in the glass and container agree well with previous measurements of the temperature histories and residual stresses. Three different thermal-stress models are developed using the finite-element method and compared. Two simple slice models were developed based on the generalized plane strain assumption as well as a detailed two-dimensional axi-symmetric model that adds elements according to the stages of pouring glass into the stainless steel container. The results reveal that mechanical interaction between the glass and the wall of the stainless steel container generates residual tensile stresses that approach the yield strength of the steel. Together, these results reveal important insights into the mechanism of stress generation in the process, the structural integrity of the product, and accuracy of the modelling-tool predictions.

1. Introduction

High-level radioactive wastes from the spent fuel of nuclear power plants must be stored safely for long time periods, in containers with completely-reliable structural integrity. High-level waste (HLW) retains 95% of its radioactivity, and can be reprocessed in the form of radioactive nitric acid solutions. This can be vitrified into a glass matrix, such as borosilicate glass, to provide a solid, stable and durable material for easier storage, transport or surveillance. HLW is stored at temporary sites, such as a solidification processing plant near the nuclear power plant, until the heat generated by the decaying fission products decreases sufficiently. Although long-term plans are yet to be decided in most countries, permanent storage of HLW as glass in containers in an underground repository is a likely strategy [1–6]. Therefore, the structural integrity of the HLW-filled containers is of critical importance to safety in both temporary and permanent storage locations.

During the casting process to pour and solidify the HLW-laden glass into stainless steel containers, residual stresses develop in the glass due to the viscoplastic flow generated by differences in cooling and temperature gradients between the center and surface of the glass. Residual stresses also arise in the steel container, due to plastic yielding caused by mismatch in shrinkage of the container walls relative to the glass. The residual stresses in the container wall are tri-axial tensile [7,8], and must not exceed the corrosion cracking threshold. In the glass, residual tensile stresses could cause cracking leading to increased leaching rate of radioactivity into the environment [9,10]. In fact, stressing and cracking of the glass is a very complex phenomenon that depends on thermal stresses as well as interaction with the container wall. Thus, to quantify the long-term structural integrity of the system, it is important to develop mathematical models to predict the temperature, deformation, strain and stress distribution in both the glass and the stainless steel container. Furthermore, the models should be validated with relevant experimental measurements.

Only a few previous models have studied thermal-mechanical behaviour of glass encapsulated in cylindrical containers [7,11]. These models are simple, one-dimensional models of a slice through the center of the process. The predicted residual stress in

* Corresponding author.
E-mail address: snakhodchi@kntu.ac.ir (S. Nakhodchi).

http://dx.doi.org/10.1016/j.ijpvp.2016.07.001
0308-0161/

Nomenclature

c_p	specific heat
D	tensor of elasticity
d_{gap}	gap length
E	Young's modulus
h	film coefficient
k	thermal conductivity
k_{eff}	effective thermal conductivity
q	heat flux
R	radius of the container
R_0	radius of the container at 20 °C
T	temperature
T_0	glass solidification temperature
T_{ref}	reference temperature
u	displacement

Greek letters

α	thermal expansion coefficient
$\dot{\varepsilon}_{el}$	elastic strain rate
$\dot{\varepsilon}_{in}$	inelastic strain rate
$\varepsilon_r(h)$	relaxed residual strain at the depth h
$\dot{\varepsilon}_{th}$	thermal strain rate
$\dot{\varepsilon}_{total}$	total strain rate
ρ	density
η	viscosity
ν	Poisson's ratio
σ	stress
$\dot{\sigma}$	stress rate
δ	displacement

Subscripts

air	related to air
ext	exterior
g	glass
θ, c	circumferential (hoop) direction
int	interior
s	steel wall
t	temperature
th	thermal
r, x_1	radial direction
z, x_2	axial direction

the glass is approximately parabolic with tension in the middle of the cross section and compression at the edges [7,11], which agrees with previous work using simple elastic models [12,13]. The pre-heated walls of the stainless steel container shrink around the glass, which causes tension to arise in the steel, and lowers all of the stresses in the glass.

Different constitutive models have been used to predict residual stresses in glass. Below the glass transition temperature, glass has an amorphous crystal structure that is solid and brittle and hardly deforms permanently, exhibiting entirely elastic behaviour [14]. The simple "instant freezing" model assumes liquid glass converts to solid instantly, and behaves elastically, ignoring stresses generated above the glass transition temperature [15]. Viscoelastic behaviour for glass was an improvement, requiring transient analysis [13,16]. Elastic – viscoplastic behaviour is a better model for glass at high temperature, in order to incorporate the strong variations in viscous flow with temperature. Example applications include glass sheet forming and deforming while cooling under its own weight [17–19] and glass molding [20]. A material model of the latter type was employed for glass in both the previous work by the current authors [11,21], and in the current research.

Relatively few previous experimental studies have measured residual stress in high level waste containers [8,11]. Pennick [8] at British Nuclear Fuels Limited (BNFL) (a predecessor company to the current UK National Nuclear Laboratory (NNL)) reported strain measurements in a full-scale container during filling operations using high temperature weldable strain gauges and laser spackle photography. Residual stresses were then determined using strain gauges via an air abrasive technique. The strain gauges showed great fluctuations during the filling and stresses increased during the cooling process. Previous measurements by the current authors are summarized in Section 3.

2. Objectives

The objective of the current research which supports ongoing studies of the damage formation in graphite [30,31] and glass [32] is to build on previous work [7,11] to better quantify and understand thermo-mechanical behaviour during the HLW-glass casting process using improved computational models. Full-scale experimental measurements were conducted previously during pouring of glass into a stainless-steel container, measuring temperatures during the process, and later determining residual stresses in the container wall [7,11]. In the current work, three different thermo-mechanical finite-element models are developed to predict temperature and stress distributions in the glass and stainless steel container and their results are compared. The results are evaluated to better understand the process, the structural integrity of the product, and the accuracy of the modelling-tool predictions.

3. Experiments

Temperature measurements were performed at the UK NNL, during the pouring of glass, used to simulate high level waste, into a 309 stainless steel container [7,11]. Fig. 1a) shows the dimensions of the container and the locations of the three thermocouples embedded into the container wall. The first step was to preheat the container to 600 °C. Then, molten glass with an initial temperature of 1050 °C was poured into the warm container in two steps. The recorded temperature histories are shown in Fig. 2a).

Residual stress measurement were performed at the University of Bristol, after it was completely cooled to ambient temperature, residual stresses were measured at 3 positions in the middle section of the wall of the stainless steel container, using the Incremental Center Hole Drilling (ICHD) technique [22,23]. The positions were spaced equally around the circumference of the container, as shown in the cross section (top view) given in Fig. 1b). Strain gauge rosettes corresponding to type 062UL were used to measure the released surface strains after each step of drilling. A RS-200 precision milling guide was combined with a 1.6 mm diameter specific purpose drill provided by Vishay Measurement Group to drill the hole. The hole was drilled in several incremental steps, starting 0.016 mm beneath the surface. Larger increments were chosen later. Residual stresses were then calculated from the measured surface strains using the integral method, as explained in detail elsewhere [7,11].

The average of the residual stresses in the hoop and axial directions were also determined and are given in Fig. 2b). Tensile

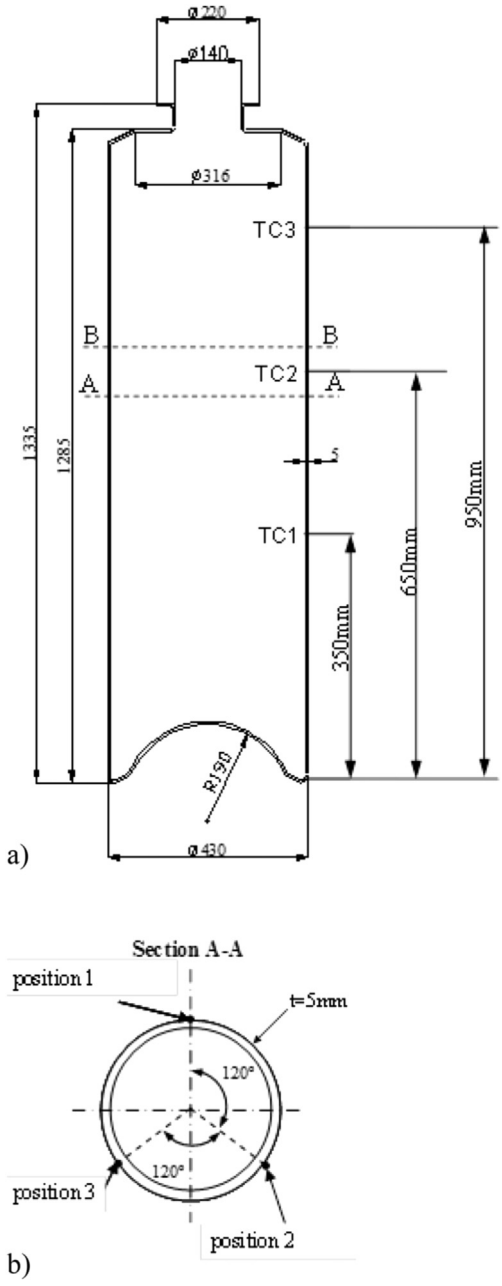

Fig. 1. a) Geometry of the steel container and location of the 3 thermocouples on the steel outer wall b) Cross section of the steel container including the residual stress measurement positions, dimensions are in mm.

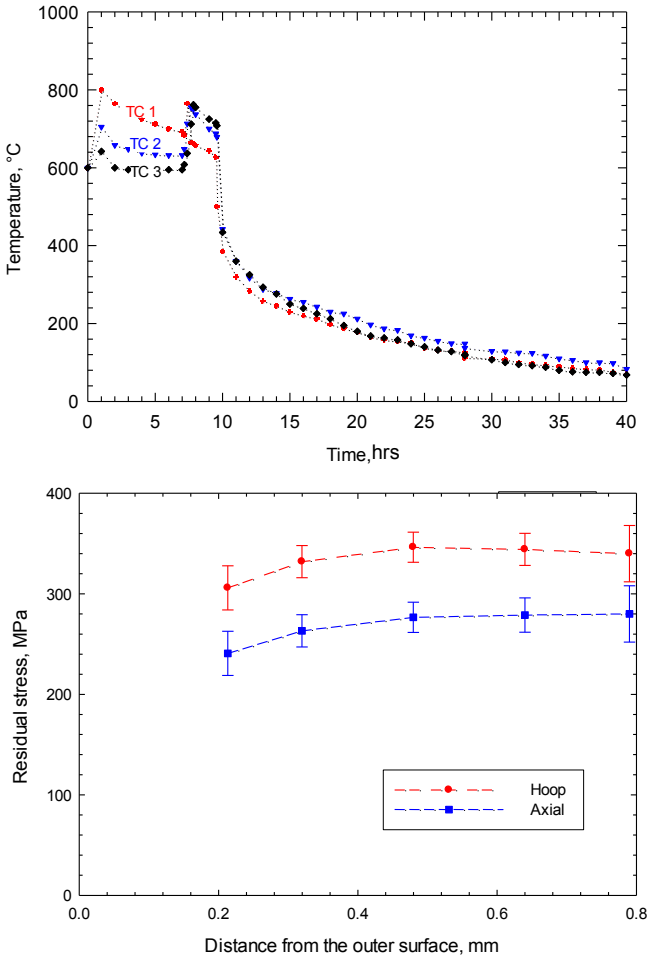

Fig. 2. Experimental measurements in steel container showing a) time-temperature histories during filling b) average residual stress [7,11].

hoop stresses varied up to approximately 350 MPa at 0.7 mm below the surface. Similarly, axial stresses were tensile throughout the wall thickness, and increase from zero at the surface to 400 MPa at 0.7 mm below the surface.

4. Thermo-mechanical finite element models

Thermal-mechanical finite-element analysis was performed to provide a quantitative description of transient temperature evolution and the generation of stresses in the solidifying glass and the stainless steel container. Three different finite-element models were developed and compared. The first two models consider a slice domain at the middle height section across the container, with an elastic-viscoplastic constitutive relation for the glass. The first slice model considers only the cooling process, and was used in previous work [11]. The second slice model includes the entire multi-step pouring and cooling process described in section 1. The third model considers a 2-D axisymmetric domain of the entire container, with a simple elastic constitutive relation. The pouring stage in this model is simulated by adding new elements of glass during each pouring step. All three models simulate the thermal and physical interaction between the glass and the container wall. The heat transfer and stress models are sequentially coupled, by first solving the transient heat conduction equation, and then reading the resulting temperatures as a predefined field into the mechanical model.

4.1. Heat transfer model

The heat transfer models all solve the transient heat conduction equation,

$$\rho C_p \frac{\partial T}{\partial t} = \frac{\partial}{\partial x_i}\left(k_{eff}\right)\frac{\partial T}{\partial x_i} \quad (1)$$

where ρ is density, C_p is specific heat, and k_{eff} is effective isotropic temperature dependant conductivity. The 1-D slice models consider only radial (x_1-direction) heat conduction (i = 1), Fig. 3a), whereas the 2-D heat transfer model, considers both radial and axial conduction (i = 1,2), Fig. 3b).

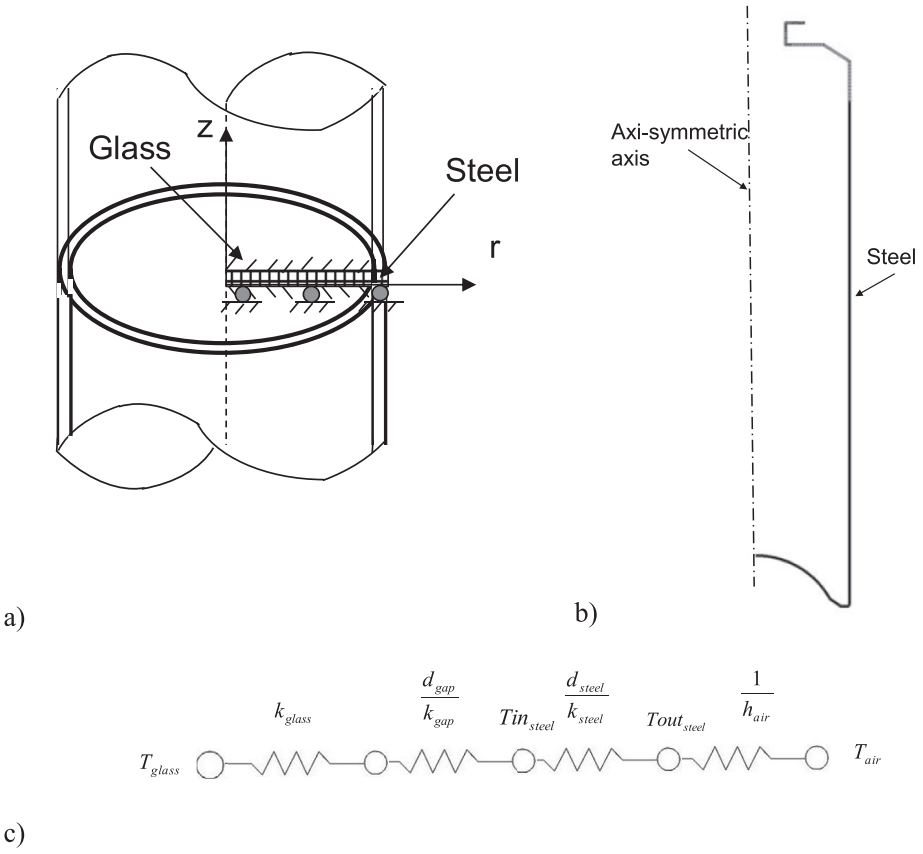

Fig. 3. Finite element domain in a) slice model b) 2-D model c) thermal resistor diagram in the slice model.

Thermal boundary conditions for the slice models are shown as a series of thermal resistors in Fig. 3, with parameter values listed in Table 1. A natural-convection boundary condition is applied at the wall exterior:

$$-k_s \left.\frac{\partial T}{\partial x}\right|_{ext} = h_{air}(T_S - T_a) \tag{2}$$

To roughly incorporate the two stages of pouring into the complete slice model 2, the ambient temperature was made to evolve from 600 °C to 500 °C to 720 °C to 570 °C, with an ambient film coefficient of 10 W/m^2 °C. This was found to produce temperature histories in the stainless steel that matched well with the thermocouple measurement at that height. Symmetry boundary conditions were imposed at the top and bottom surfaces by assigning q = 0 at the glass central axis and by neglecting the small temperature gradient in the axial direction, z, as illustrated in Fig. 3a). During cooling, the ambient temperature was dropped to 25 °C keeping the film coefficient 10 W/m^2 °C. Heat flux across the interface between the glass exterior and steel-wall interior is:

$$q = -k_g \left.\frac{\partial T}{\partial x}\right|_{ext} = k_s \left.\frac{\partial T}{\partial x}\right|_{\text{int}} = \frac{k_{air}}{d_{gap}}(T_s - T_g) \tag{3}$$

After filling is completed, heat leaves the exterior surface of the glass, conducts across the glass-wall interface, and conducts through the steel wall. Some of this heat flux causes the steel wall to heat up, and the rest of the heat conducts through the wall to be lost from the wall exterior surface by convection and radiation with the ambient air. Heat transfer across the interfacial gap is controlled by a contact resistance, according to the microscopic (roughness) and macroscopic (waviness) features of the surfaces, and the conductivity of the material (air) in the gap [24]. Consequently, there is a temperature drop across the gap. The contact resistance depends on temperature and pressure [25]. In addition to the gap thickness, a temperature-dependant contact resistance was adopted in this model based on air at the average temperature of the two surfaces. Specifically, the gap in this work, d_{gap}, is 0.1 mm thick with conductivity varying from 0.032 W/m^2 °C (at 200 °C) to 0.068 W/m^2 °C (at 1400 °C) [25].

Similar thermal boundary conditions have been previously implemented in simulations of static-cast steel ingots [26]. The sensitivity of the model to the thermal contact conductance is investigated and discussed in section 5. During the pouring stage, some heat may be radiated from the rising top surface of the glass pool to the unexposed upper interior container wall, but this effect was considered small and neglected.

Table 1
Heat Transfer model parameters.

Glass initial temperature, T_{glass} (°C)	1050
Glass conductivity, k_g, (Wm^{-1} K^{-1})	1.1–1.3
Gap conductivity, k_{gap} (Wm^{-1} K^{-1})	0.032–0.068
Gap thickness, L_{gap} (m)	0.01
Steel conductivity, k_s, (Wm^{-1} K^{-1})	15–19
Specific heat of glass (J/kg°C) (<100 °C)	830
Specific heat of glass (J/kg°C) (>500 °C)	1300
Steel initial temperature, T_{steel} (°C)	600
Steel thickness, L_{steel} (m)	0.005
Air heat transfer coefficient, $h_{ambient}$ (Wm^{-2} K^{-1})	10

The temperature Tg in Eq. (3) changes with time from 1050 °C to 30 °C according to when the glass level passes any given height up the container.

More realistic boundary conditions were implemented into the 2-D model. Using the element-birth technique and "model change" option in ABAQUS software, glass elements were added in two steps, representing the two pouring steps during the experimental procedure, as explained in section 3. The first pouring step lasted 3600 s and was simulated by incrementally adding the ambient temperature of 650 °C and ambient film coefficient of 90 W/m^2 °C. The second pouring step was simulated similarly by adding five additional increments of 720 s. During this period and between the two pouring steps, the ambient temperature was 600 °C and the film coefficient to 50 W/m^2 °C. After removal from the furnace, final cooling was modelled by dropping the ambient temperature to 25 °C and the film coefficient to 15 W/m^2 °C. With this Lagrangian formulation, temperatures, mechanical strains and stresses continually evolve during all of these stages.

4.2. Stress model

The domains for the slice and 2-D axisymmetric stress models are shown in Fig. 3a and b respectively. In each time step, the temperature field calculated from the heat transfer analysis is input as a predefined field into the corresponding stress model.

The mechanical analysis step involves solving the equilibrium equations, constitutive equations and compatibility equations, which relate force to stress, stress to strain and strain to displacement respectively. In the Lagrangian frame appropriate for this work, the force equilibrium balance given below is the general governing equation for the static-mechanics problem,

$$\nabla \cdot \sigma_{ij} + \rho g h = 0 \tag{4}$$

Where σ_{ij} is the stress tensor, the second term represents the body force from the hydrostatic pressure due to gravity of g and the height of molten glass, h, above the simulated slice. As shown in the Appendix, the hydrostatic pressure is negligible compared to the measured stresses. Thus, the difference between slices at different heights is negligible mechanically and so the assumption of a state of generalized plane-strain in a single slice is reasonable. The compatibility equations to relate strains and displacements are given by:

$$\dot{\varepsilon} = \frac{d}{dt}\left[\frac{1}{2}\left(\nabla \boldsymbol{u} + (\nabla \boldsymbol{u})^T\right)\right] \tag{5}$$

where $\boldsymbol{u}$ is the displacement vector.

For the constitutive equation for the grade 309 stainless steel container, elastic perfectly-plastic behaviour was assumed. The temperature-dependant Young's modulus used in this model was fitted to the experimental data provided by NNL [29] and is shown in Fig. 4b) along with temperature dependent yield stress of stainless steel. A constant Poisson ratio of 0.3 was assumed.

In the glass, the strain-rate dependent constitutive behaviour was treated as a transient solidification process, dividing the total strain rate into three components of elastic strain rate, $\dot{\varepsilon}_{el}$, thermal strain rate, $\dot{\varepsilon}_{th}$, and inelastic strain rate:

$$\dot{\varepsilon}_{total} = \dot{\varepsilon}_{el} + \dot{\varepsilon}_{th} + \dot{\varepsilon}_{in} \tag{6}$$

Elastic strain is directly responsible for stress, which is defined as follows for a linear material with negligible large rotations.

$$\dot{\sigma} = D : (\dot{\varepsilon}_{toal} - \dot{\varepsilon}_{th} - \dot{\varepsilon}_{in}) \tag{7}$$

where D is the 4th-order tensor of elastic constants, characterized here for an isotropic material by the temperature-dependent elastic modulus, given in Table 2 and shown in Fig 4b), and a constant Poisson ratio for glass, 0.2.

4.2.1. Thermal strain

Thermal strains are found from the temperature field calculated by the heat transfer model. They arise due to volume changes caused by temperature differences.

$$\varepsilon_{th} = \int_{T_{ref}}^{T} \alpha(T) dT \tag{8}$$

where α is the average coefficient of thermal expansion between the reference temperature, T_{ref}, and temperature, T, and is given in Table 2 for the glass and in Table 3 as a function of temperature for the 309 steel, based on a reference temperature of 20 °C.

4.2.2. Visco-plastic strain

Inelastic or "viscoplastic" strain includes indistinguishable parts of strain-rate independent plasticity and time-dependant creep. The constitutive equation for glass is obtained from Newtonian incompressible behaviour, relating inelastic strain to stress in the glass as follows:

$$\sigma = 3\eta(T)\dot{\varepsilon}_{in} \tag{9}$$

where σ is stress, η is the temperature-dependant viscosity and $\dot{\varepsilon}_{in}$ is the inelastic strain rate.

Viscosity data for borosilicate glass [27] were fitted to the following equation [28].

$$\log \eta = A + \frac{B}{T - T_0} \tag{10}$$

where A = 0.5, B = 2593 and T_0 = 374.8 are empirical fitting constants.

In Eqs. (9) and (10), as temperature decreases, viscosity increases until it reaches the solidification temperature, T_0. Simple elastic behaviour with an initial strain was applied at temperatures below the solidification temperature, where the inelastic strain rate dropped to zero.

4.2.3. Boundary conditions

Mechanically, the slice models are subjected to the generalized plane strain condition in the axial direction, in order to properly account for axial stress the vertical displacement, z direction in Fig. 3a), at the top of the slice models was coupled.

5. Comparison of finite-element models with experiments

5.1. Temperature

The temperature histories predicted by the slice models are compared with those measured at the exterior surface of the stainless steel container in Fig. 5. Fig. 5b) compares the original slice model 1 cooling stage results only. Fig. 5c) compares the slice model 2 which includes the pouring stage as well. The difference between internal and external temperatures across the steel container wall was very small, owing to its high thermal conductivity and small thickness. Thus, only the exterior temperature is shown. The

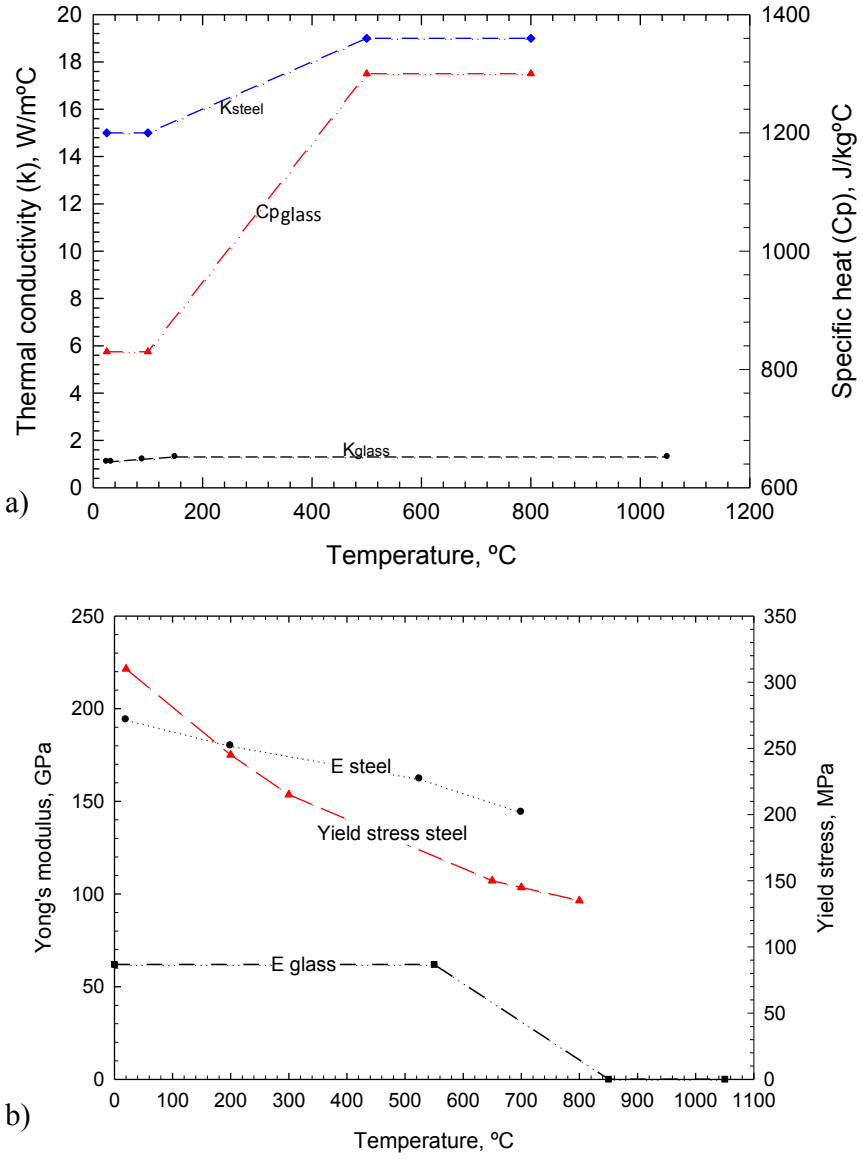

Fig. 4. Temperature dependant a) thermal and b) mechanical properties of stainless steel and glass.

Table 2
Mechanical properties of glass.

Parameter	Value
E_{glass} (GPa) in solid state (<525 °C)	62
E_{glass} (GPa) in liquid state (>850 °C)	1
Density, ρ (kg/m^3), in solid state	2400
Density, ρ (kg/m^3), in liquid state	2200
Thermal expansion coefficient of glass (m/m)	3.2×10^{-6}

Table 3
Temperature-dependant thermal expansion coefficient of steel.

Thermal expansion coefficient of steel (m/m)	Temperature, °C
1.6×10^{-5}	200
1.7×10^{-5}	400
1.8×10^{-5}	600
1.85×10^{-5}	800
1.95×10^{-5}	1000

temperature history predicted in the steel container agrees with the thermocouple measurements.

The temperature predictions of the 2-D model are shown in contour plots at different times during pouring in Fig. 6. Fig. 7 shows temperature histories at the 3 locations of the thermocouples in the steel wall, which agree well with the measurements. Of particular interest is the temperature evolution at the exterior surface of the glass. The model and measurements in these figures produce the same insights into the process, which are discussed in detail in the discussion section.

The steel wall temperature depends mainly on the resistances from the gap and from convection to ambient, according to the resistor model in Fig. 3c). The gap resistance changes greatly with ambient temperature and convection coefficient, h and t, which can change the direction of the heat flux. For example, a sudden decrease in gap resistance may cause an increase of temperature of the steel wall. On the other hand, having a fixed gap resistance, ambient resistant, h and t, controls the temperature of the steel. The latter is used to simulate the pouring process.

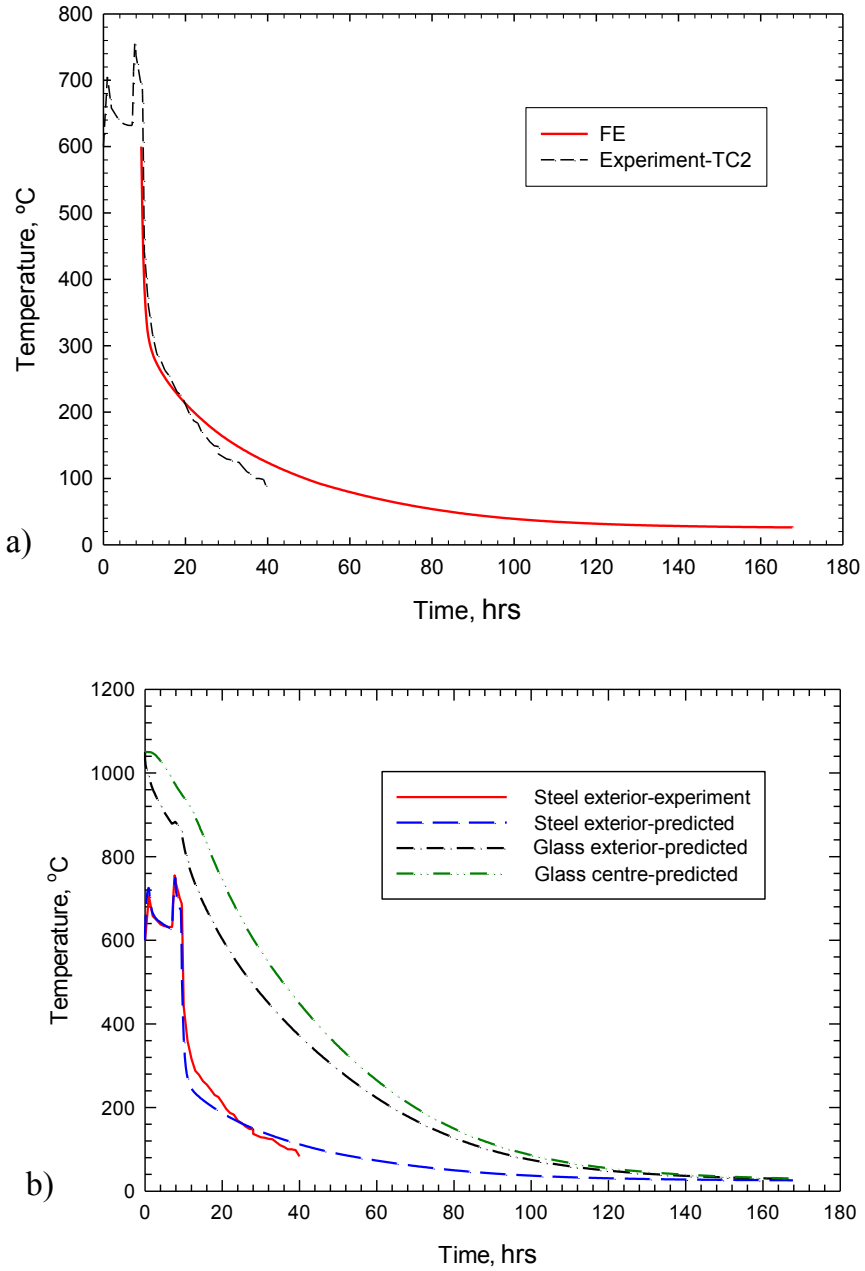

Fig. 5. Temperature distributions calculated by heat transfer slice models compared with measurements for a) slice model 1 and b) slice model 2.

5.2. Stress

The stress distributions obtained from the all three models are compared with the residual stress measurements in the wall of the stainless steel container in Figs. 8 and 9 in both the hoop and axial directions. The final hoop residual stress distribution in the glass is also zoomed-in and shown in Fig. 8. All three models predict hoop residual stresses that are tensile in the center of the glass, compressive near the glass and steel interface, and tensile in the container wall.

There is good agreement between the residual stress predictions and the measurements. The slice model with cooling underestimates the final residual hoop stress measurements by ~15%. The slice model with both pouring and cooling is slightly better, underestimating the measurements by only ~10%. None of the slice models predict the high axial residual stresses in the container. The full 2-D model over-predicts the hoop stress by 5%, as shown in Fig. 9. This model correctly predicts that the axial stress is less than the hoop stress. However, the predicted axial stress is much less than the measurement.

Stress profiles during the transient cooling process are presented in Fig. 10, for the slice model with cooling only. To quantify the importance of the mechanical interaction between the glass and the container, a simulation was conducted with no constraint/contact between the glass and steel in the same slice model. The results are included in Fig. 10 for comparison.

During the initial cooling process, the surface region of the glass cools faster than its center. As shown in Fig. 10a) for the non-contact case, the resulting surface contraction causes very slight compression stress at the center, balanced by slight tension near

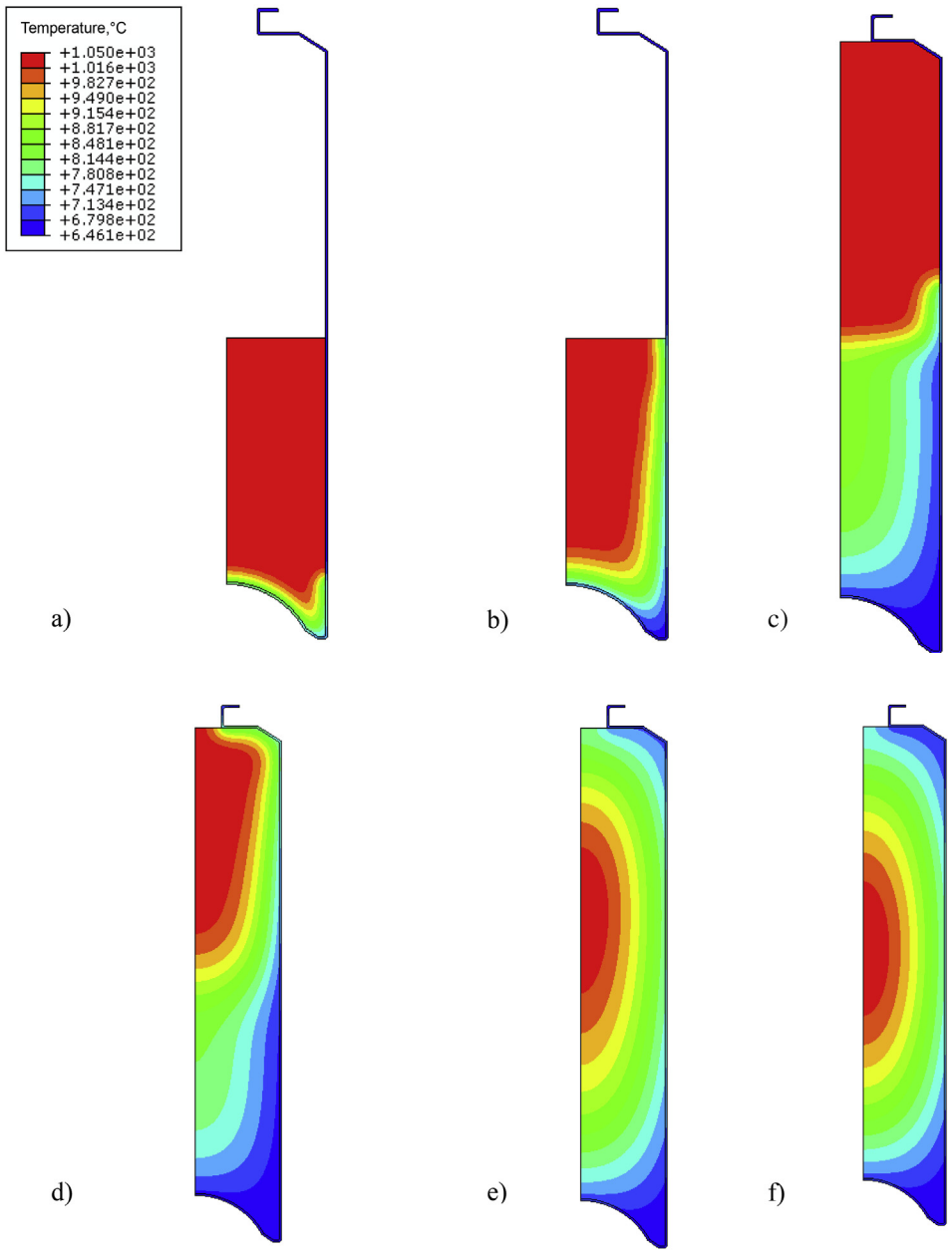

Fig. 6. Temperature distributions in glass calculated by 2-D model at different times, a) 720 s, b) 3600 s c) 26700 s d) 32100 s e) 86100 s f) 172100 s.

the surface. A similar balanced stress profile develops in the steel wall. This situation might happen if the steel cylinder were not preheated, and the expansion of the steel wall caused by heating during the pouring stage results in gap formation between the steel and glass. Including mechanical contact for the real process, however, the cooling contraction of the steel wall is much greater than that of the glass. Thus, the steel wall squeezes the entire glass volume into compression, which is balanced by high tension stress throughout the steel wall.

Later during cooling, Fig. 10b) shows results at 31500s, when the glass center is 900 °C and exterior is 730 °C, and Fig. 10c) shows results at 45900s, when the glass center is 800 °C and the exterior is 650 °C. Even with no contact, the natural cooling and contraction of the soft center of the glass within the strong, cold, solidified surface shell of glass causes the stress profile to reverse. The hoop stresses towards the center rise to zero and later become tensile. This is balanced by compressive stress developing within the exterior. This trend continues until in Fig. 10d) where the glass is cooled to the room temperature and hoop residual stresses reach 10 MPa tension at the center of the glass and 20 MPa compression at the exterior. The residual stress in the steel wall ultimately drops to zero, for this case without contact.

With mechanical contact included, Fig. 10 also shows that the wall of the stainless steel container shrinks to push on the glass during all times of the cooling process. This generates the high stresses in the steel wall. The tensile hoop stresses in the stainless steel wall container develop solely as a result of mechanical interaction with the glass. Specifically, the mechanical interaction generated about 150 MPa hoop stresses in Fig. 10a) that increased to about 220 MPa, 240 MPa and 305 MPa in Fig. 10a,b and c)

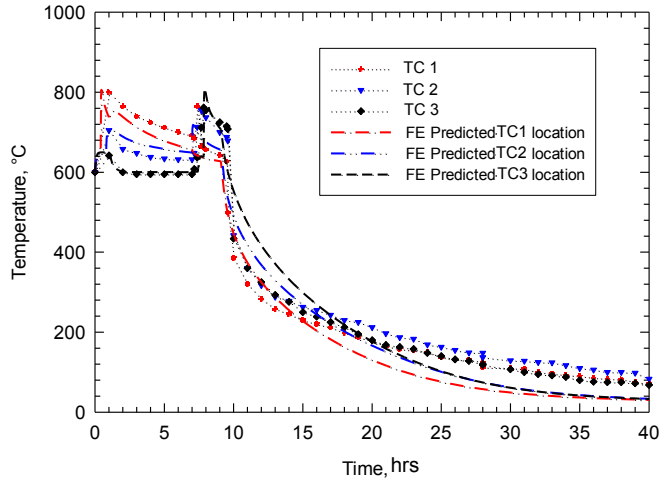

Fig. 7. Comparison between experimental thermocouple readings in the steel container wall and 2-D finite element model predictions.

respectively. Compressive stress in the glass is higher towards the surface because the region is colder and stronger.

Finally, Fig. 10d) shows that the residual hoop stresses in the glass are always tensile at the center and compressive at the surface. With mechanical interaction, however, the residual tensile stress in the glass center rises to only ~4 MPa by. Thus, as discussed in further detail later, the process of preheating the steel cylinder ultimately lowers the internal tensile stress inside the glass, at the expense of residual tensile stress in wall itself.

Results obtained from the more realistic geometry of the 2-D model are shown in Fig. 11. Fig. 11 shows the displacement histories of the outer surface of the glass and inner surface of the container wall for this case. During the pouring stage, the first 10 h, radial displacement of steel experienced a sharp increase followed by a decrease to its initial value at the start of the process. Comparing the results presented in Fig. 11 with the temperature histories presented in Fig. 7, pouring increased temperature and its consequences on the radial displacement can be seen. Note that the steel expand faster than the glass, owing to the larger thermal expansion coefficient of the steel (relative to the glass). This causes a separation between glass and steel during the first 10 h in Fig. 11. This non-physical result demonstrates that in reality, the molten glass follow the shape of the container until steel return to its initial radius at the start of the process. Then, the container wall will shrink until it contacts the glass. The initial radius of the container (when pouring started at time = 0) is larger than its final radius at the ambient temperature, due to thermal contraction. Cooling the container causes its radius to return to its original value at room temperature until the wall hits the glass. In section 6.2, radial displacement of the container correspond to the measured residual stresses is calculated (see Fig. 12).

6. Discussion

Numerical models are efficient tools to elucidate thermal and mechanical stress generation and cracking in complex engineering processes. The simple models can produce realistic results if formulated properly. The measurements and calculations in this work together provide new insight into thermo-mechanical behaviour during casting processes, such as the pouring, cooling and storage of HLW-glass in a cylindrical steel container. This can aid in the design and operation of these processes. Most of the stresses in a static casting process are generated from volumetric contraction and expansion associated with changing thermal gradients within the mold [26,29]. In addition, the casting (glass) and mold (stainless steel container) are in both thermal and physical contact, which changes the cooling rates, and redistributes the

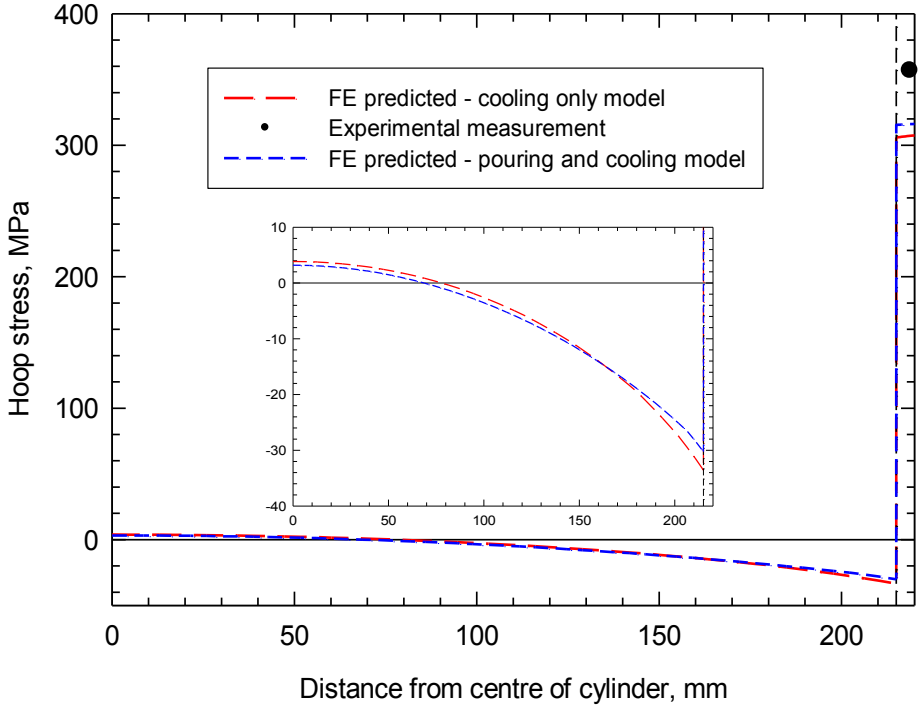

Fig. 8. Comparison between residual stress measurement and FE stress prediction in the slice models.

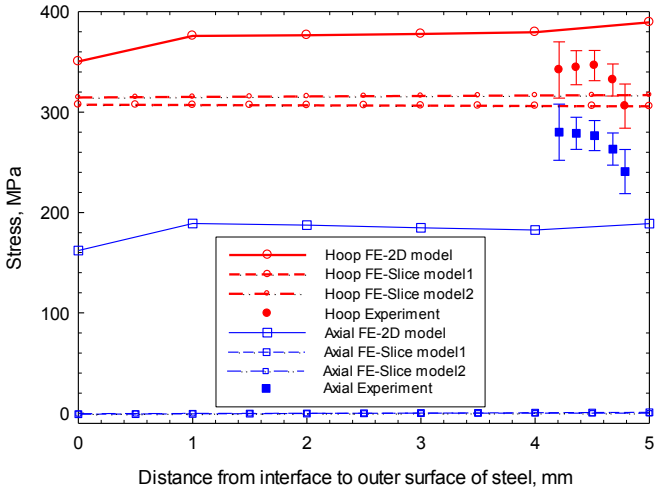

Fig. 9. Comparison between FE predicted hoop and axial stress with residual stress measurement.

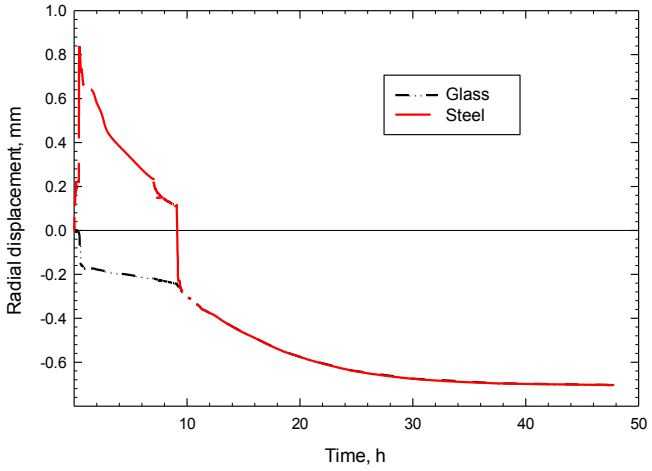

Fig. 11. Displacement histories of the steel in detailed 2-D model.

internal stresses, according to their relative contractions or expansions. Three FE models were developed in this research, the first two FE models were developed from a slice domain from middle of the container through the glass and steel. These two simple but efficient models simply reveal the process of stress development in

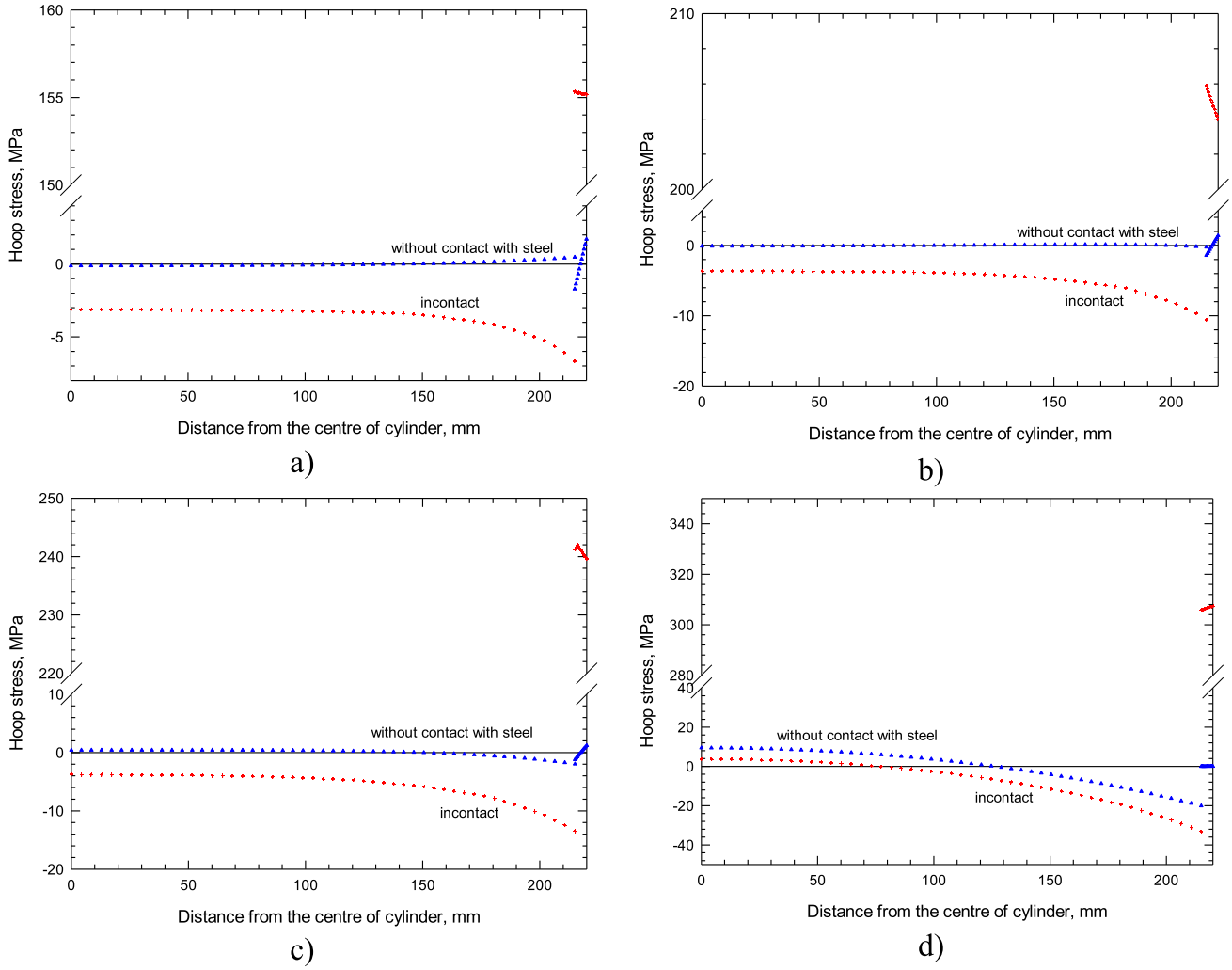

Fig. 10. Stress state in glass and steel in the "cooling only" slice model with and without physical interaction between glass and steel a) time = 15300 s, $T_{g\text{-centre}}$ = 1010 °C, $T_{g\text{-exterior}}$ = 850 °C b) time = 31500 s, $T_{g\text{-centre}}$ = 900 °C, $T_{g\text{-exterior}}$ = 730 °C c) time = 45900sec, $T_{g\text{-centre}}$ = 800 °C $T_{g\text{-exterior}}$ = 650 °C d) time = 600000, $T_{g\text{-centre}}$ = 25 °C $T_{g\text{-exterior}}$ = 25 °C.

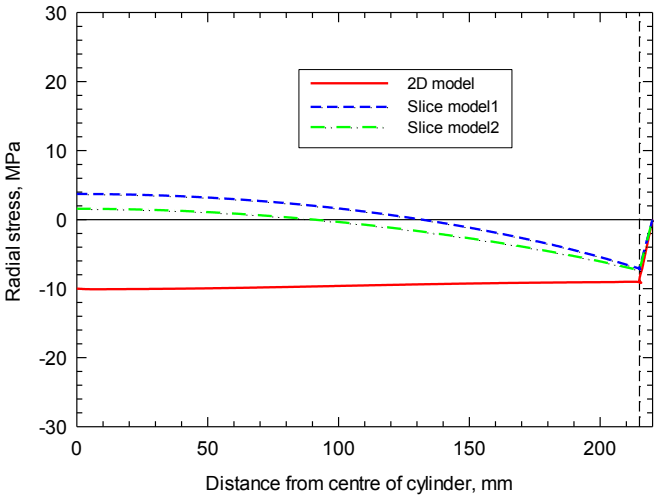

Fig. 12. Radial stresses in the FE models.

the glass and the container. It is demonstrated that the measured residual stresses in the container are caused by the thermo-mechanical contact between glass and the steel container. Comparing the residual stresses predicted by two slice models, the simple slice model of cooling process only is shown to be very efficient for predicting the residual hoop stress.

The 3rd model considers a 2D axisymmetric domain of the entire container. This model can predict both the measured axial and hoop residual stresses. Like the hoop stresses, the axial stresses are generated due to physical contact between the solidified glass and the container. The underestimation of axial stresses by the FE model may be associated with possible friction between the steel and glass during the cooling process which has not been considered in the FE model.

The section below attempt to explain further the process phenomena based on the findings in the FE models. These thermal stress models are powerful prediction tools for design and assessment of structural integrity of HLW containers.

6.1. Explanation of process phenomena

The process can be split into the three stages of preheating, pouring, cooling, and storage.

6.1.1. Preheating

Prior to filling it with molten glass, the empty stainless steel container is exposed to a certain temperature, (600 °C in this work). During this stage, the empty container is free to expand in all directions, increasing in both diameter and height. Relatively little stress is generated during preheating the container, due to its thin walls and lack of temperature gradients or constraint. It is important to achieve uniform preheating everywhere, including the container bottom, in order to avoid local temperature variations and the associated stresses, inelastic strains, and complications. Although stress is small after this stage, the thermal strains and displacements are very significant. The amount of thermal expansion increases with increasing preheat temperature.

6.1.2. Pouring

During this stage, the container is filled with liquid. Molten glass with a high initial temperature (1050 °C in this work) flows into the container and takes on its internal shape. During the flow recirculation in the liquid pool, its internal heat is generally homogenized. Some heat is conducted to the adjacent container wall it contacts, and some heat from the rising free surface is radiated to heat the upper regions of the container walls. This heat increases the temperature of the container, (especially in the bottom filled portion), causing the wall to further expand.

The changes in temperature measured by different thermocouples attached to the container walls can be explained by filling and 2-D heat conduction in the walls, according to the two time intervals of pouring molten glass into the container. Each time glass is poured into the container, the temperature of all thermocouples increases, owing in part to heat conducting vertically up the wall. The sharp temperature increase causes sudden expansion of the container wall, which could allow a gap to form, while the glass slowly expands to fill the gap. At the same time, the gap decreases the heat flux, causing the wall to stop expanding, resulting in a relatively slow cooling of the wall.

During the first pouring step, the temperature increase is highest towards the bottom of the cylinder (TC1). After the first pouring step of ~1hr, the glass and wall cool, so temperature drops slowly for the next ~6 h. During this time, the furnace heater maintains a high ambient temperature (~600 °C), which keeps the upper part of the container warm until the start of the next filling cycle at ~7hr. Then, during the second step of pouring, temperature spikes again, but only in the upper half of the wall, (especially at TC3). Again, this filling step lasted about 1hr, generating peak temperatures at ~8hr, For the next ~2 h, cooling proceeds at about the same rate as after the first pour. Then, at ~10hr, the heater was switched off or the container was removed from the furnace. The exposure to the cooler ambient temperature causes the cooling rate to greatly increase, as indicated by the sharp drop in temperature of all three thermocouples.

To contain the molten glass, a slight tensile hoop and axial stress (half as much) is needed to balance the hydrostatic pressure. However, this stress is negligible relative to the stresses caused by the mechanical and thermal strains, as shown in the Appendix.

6.1.3. Cooling

At the end of pouring, the system cools down in a transient manner. Inside the container, the glass is still soft, so it flows, generating inelastic strain, to match the shape of the cylinder wall. The latent heat released during glass solidification has a small effect to delay cooling. More important is the increase in viscosity that accompanies glass cooling, culminating in the prevention of flow upon cooling below the glass transition temperature. This cooling occurs first at the outer surface layer of the glass, strengthens this outer layer enough to contain the inner pressure. After this time, the rigid solid glass shell can shrink, so the glass no longer follows the shape of the container.

During the cooling stage, both the container and glass shrink. However, as the thermal expansion of the steel is almost three times bigger than that of the glass, the wall shrinks three times more than the glass, so it contracts around the glass everywhere. As the steel tries to shrink more, it pushes on the solid glass. If the solid glass is cold enough, it will resist this attempt to deform it smaller, and cause hoop stress: *compression in the glass is balanced by hoop tension in the container wall.*

The model predicts that the hoop stress is about two times bigger than the axial stress (Fig. 9). Although this agrees with the Appendix equations for a thin wall cylinder subjected to internal pressure, this is believed to be a coincidence. Furthermore, the measured hoop and axial stresses are almost equal. The difference may due to one or all the following reasons. 1-Friction between glass and steel 2- Pressure from bottom and lid 3- Temperature gradients in the wall.

6.1.4. Practical implications of preheating

Based on the results presented here, preheating may be beneficial in three ways: 1- Preheating will avoid high deformations due to thermal shock at the start of pouring. Without preheating, the container that is at room temperature will suddenly be exposed to the glass at 1050 °C. The high thermal gradients between the glass and the wall at the contact region could generate a thermal shock for both materials. Surface tension and cracks in the glass are the most probable. Moreover, touching a cold stainless steel wall with a hot molten glass, the rapid thermal expansion of the wall, causes a gap to be formed at the interface between the glass and the wall. If the gap formed before the glass surface layer was strong enough to withstand the internal pressure from the molten glass interior, then again surface tension and surface cracks could form. By starting already partly expanded, the steel wall does not expand as much when the glass hits it. This lessens the chance for cracks in the glass due to trying to follow that expansion. 2- Without preheating, the hot glass might be frozen at the first instant when it is in contact with the cold stainless steel container. Hence, glass would not be able to follow the shape of the container anymore. Further expansion of the container would cause gap formation, surface tension in the glass, and perhaps cracks. Keeping the container above the glass transition temperature ensures that the glass is always able to flow to conform to the shape of the container without cracking. 3- Finally, by expanding before the glass contacts it, the glass takes on a larger diameter, and thus is compressed when the wall later shrinks back to room temperature. This general compression is beneficial, as it discourages the formation of cracks in the glass.

To offset these 3 benefits, the preheating is ultimately responsible for the residual tensile stress in the walls of the container. This likely increases the chances of corrosion cracking or other long-time failure of the steel vessel. Thus, steps should be taken to alter the preheating or other aspects of the process in order to decrease this residual tensile stress in the steel wall.

7. Conclusions

- Three different thermo-mechanical FE models are developed: two simple but efficient slice models and one 2D axisymmetric model created from the full geometry of the container. All FE models include the glass and steel container along with their thermo-physical contact.
- The two slice models benefit from simplicity in modelling and provide basic knowledge of stress generation during the casting of the glass into stainless steel container.
- Of the two slice models, the model that considers cooling only is sufficiently accurate to predict the hoop stresses in the stainless steel wall container.
- The full 2-D FE model of the axisymmetric geometry takes advantage of advanced features in FE simulation and introduces the details of the glass filling and casting process by adding layers of glass and transient thermo-mechanical contact. This model confirms the general findings of the two slice models and demonstrates the axial residual stresses in the steel container are developed as a result of physical contact between the glass and the steel container in the axial direction. The presence of friction between the glass and the steel containment may lead to higher than predicted axial residual stresses. Without friction the predicted axial stresses are lower than the measured stresses.

Appendix 1. Hoop stress due to hydrostatic pressure of the molten glass

The effect of hydrostatic pressure from the molten glass to the stainless steel container can be obtained as follows,

$$P = \frac{\rho g h}{2} \tag{A1}$$

where $\rho = 2200$ kg/m^3 is the molten glass density, g = 9.8 m/s^2 is gravity and h = 1.3 m is the height of the container.

Considering the container as a thin wall cylinder, hoop stress due to hydrostatic pressure, *P*, can be calculated as follows,

$$\sigma_\theta = \frac{pr}{t} \tag{A2}$$

where $p = 0.014$ MPa is calculated pressure using equation (A1), r = 215 mm is container radius and t = 5 mm is the thickness. The final hoop stresses is $\sigma_\theta = 0.6$ *MPa* that is only 0.1% of total stress. Thus, molten glass hydrostatic pressure can be neglected.

References

[1] Deokattey S, Jahagirdar PB, Kumar V, Bhaskar N, Kalyane VL. Borosilicate glass and synroc R&D for radioactive waste immobilization: an international perspective. JOM J Minerals, Metals Mater Soc 2003;55:48–51.
[2] Donald IW, Metcalfe BL, Taylor RNJ. The immobilization of high level radioactive wastes using ceramics and glasses. J Mater Sci 1997;32(22):5851–87.
[3] Hidekazu A, Masanori A. Long-term integrity of waste package final closure for HLW geological disposal, (I) points at issue concerning 1,000 Years Containment capability of overpack. J Nucl Sci Technol 2005;42(5):470–9.
[4] International Atomic Energy Agency. The long-term storage of radioactivity waste:safety and sustainability. In: Technical committee meetings. Vienna, Austria: IAEA; 2002.
[5] Lam P-S, Sindelar RL. Flaw stability considering residual stress for aging management of spent nuclear fuel multiple-purpose canisters. J Press Vessel Technol 2016;138. 041406.
[6] Lam P-S, Sindelar RL, Duncan AJ, Adams TM. A framework to develop flaw acceptance criteria for structural integrity assessment of multipurpose canisters for extended storage of used nuclear fuel. In: ASME 2014 Pressure Vessels and Piping Conference; 2014. pp. V06AT06A019-V06AT06A019.
[7] Nakhodchi S. Prediction and measurement of strains and stresses in metallic and non-metallic materials. PhD Thesis, Mechanical Engineering. Bristol: University of Bristol; 2009.
[8] Pennick AM. Summary of stress measurements made on glass containers in the full scale inactive plant(1984-1986). BNFL; 1987. p. 6.
[9] Kamizono H, Senoo M. Thermal shock resistance of a simulated high-level waste glass. Nucl Chem Waste Manag 1983;4(4):329–33.
[10] Peters RD, Slate SC. Fracturing of simulated high-level waste glass in canisters. Nucl Eng Des 1982;67(3):425–45.
[11] Nakhodchi S, Thomas BG, Smith DJ. Modeling and measurement of residual stresses in a steel vessel containing glass. ASME J Eng Mater Technol 2011:133.
[12] Aben H, Guillemet C. Photoelasticity of glass. Springer-Verlag; 1993.
[13] Carre H, Daudeville L. Numerical simulation of soda-lime silicate glass tempering. J Phys IV Fr 1996;06(C1). p. C1-175–C1-185.
[14] Budinski KG, Budinski MK. Engineering materials properties and selection. Prentice Hall; 2005.
[15] Indenbom VL. A theory of glass annealing. Zhurnal Sakharnoi Promyshlennosti 1954;24:925–8.
[16] Narayanaswamy OS. Stress and structural relaxation in tempering glass. J Am Ceram Soc 1978;61(3–4):146–52.
[17] Parsa MH, Rad M, Shahhosseini MR, Shahhosseini MH. Simulation of windscreen bending using viscoplastic formulation. J Mater Process Technol 2005;170(1–2):298–303.
[18] Moreau P, Lochegnies D, Oudin J. An inverse method for prediction of the required temperature distribution in the creep forming process. Proc Institution Mech Eng Part E J Process Mech Eng 1998;212(1):7–11.
[19] Locheginies D, Moreau P, Oudinn J. Finte element strategy for glass sheet manufacture by creep forming. Communivation Numer Methods Eng 1996;12:331–41.
[20] Yi AY, Jain A. Compression molding of aspherical glass lenses–a combined experimental and numerical analysis. J Am Ceram Soc 2005;88(3):579–86.
[21] Koric S, Thomas BG. Efficient thermo-mechanical model for solidification processes. Int J Numer Methods Eng 2006;66(12):1955–89.

[22] Hilson G, Simandjuntak S, Flewitt PEJ, Hallam KR, Pavier MJ, Smith DJ. Spatial variation of residual stresses in a welded pipe for high temperature applications. Int J Press Vessels Pip 2009;86(11):748–56.
[23] Stefanescu D, Truman C, Smith D, Whitehead P. Improvements in residual stress measurement by the incremental centre hole drilling technique. Exp Mech 2006;46(4):417–27.
[24] Zhu H. Coupled thermal–mechanical finite-element model with application to initial solidification. In: Department of mechanical and industrial engineering. USA: Urbana: University of Illinois; 1993.
[25] Park JK, Thomas BG, Samarasekera IV. Analysis of thermomechanical behaviour in billet casting with different mould corner radii. Ironmak Steelmak 2002;29(5).
[26] Thomas B, Samarasekera I, Brimacombe J. Mathematical model of the thermal processing of steel ingots: Part I. Heat flow model. Metallurgical Mater Trans B 1987;18(1):119–30.
[27] Anurag J, Gregory CF, Allen YY. Viscosity measurement by cylindrical compression for numerical modeling of precision lens molding process. J Am Ceram Soc 2005;88(9):2409–14.
[28] Fulcher GS. Analsis of recent measurement of the viscosity of glasses. J Am Ceram Soc 1925;8(6):339–55.
[29] Thomas B, Samarasekera I, Brimacombe J. Mathematical model of the thermal processing of steel ingots: Part II. Stress model. Metallurgical Mater Trans B 1987;18(1):131–47.
[30] Nakhodchi S, Flewitt P, Smith D. A method of measuring through-thickness internal strains and stresses in graphite. Strain 2011;47:37–48.
[31] Nakhodchi S, Smith DJ, Flewitt PEJ. The formation of fracture process zones in polygranular graphite as a precursor to fracture. J Mater Sci 2013;48:720–32.
[32] Nakhodchi S, Hilson G, Smith DJ, Flewitt PE. A consideration of the measurement of macro-stresses in non-metallic materials. Key Eng Mater 2010: 221–4.